https://doi.org/10.5194/essd-2021-1
Preprint. Discussion started: 8 February 2021

Open Access Earth System Science Data Discussions

A synthesis dataset of permafrost thermal state for the Qinghai-Xizang (Tibet) Plateau, China

Lin Zhao[1,2*], Defu Zou[2], Guojie Hu[2*], Tonghua Wu[2], Erji Du[2], Guangyue Liu[2], Yao Xiao[2], Ren Li[2], Qiangqiang Pang[2], Yongping Qiao[2], Xiaodong Wu[2], Zhe Sun[2], Zanpin Xing[2], Yu Sheng[3], Yonghua Zhao[2], Jianzong Shi[2], Changwei Xie[2], Lingxiao Wang[1], Chong Wang[1], Guodong Cheng[2]

[1] *School of Geographical Sciences, Nanjing University of Information Science & Technology, Nanjing 210044, China*

[2] *Cryosphere Research Station on Qinghai-Xizang Plateau, State Key Laboratory of Cryospheric Sciences, Northwest Institute of Eco-Environment and Resources, Chinese Academy of Sciences, Lanzhou 730000, China*

[3] *State Key Laboratory of Frozen Soil Engineering, Northwest Institute of Eco-Environment and Resources, Chinese Academy of Sciences, Lanzhou 730000, China*

Correspondence: Lin Zhao (lzhao@nuist.edu.cn), Guojie Hu (huguojie123@lzb.ac.cn)

Abstract:

Permafrost is important for the climatic, hydrological, and ecological processes on the Qinghai-Xizang (Tibet) Plateau (QXP). The changing permafrost and its impact have been attracting great attention worldwide never before, and more observational and modeling approaches are need to promote an understanding of permafrost thermal state and climatic conditions on the QXP. However, there were almost no synthesis dataset on the permafrost thermal state and climate background on the QXP, but were sporadically reported in different literatures due to the difficulties to access to and work in this region, where the weather is severe, and environmental conditions are harsh and the topographic and morphological features are complex. In this study, a comprehensive dataset under quality controlled consisting of long-term meteorological, ground temperature, soil moisture and soil temperature data were compiled from an integrated, distributed and multiscale observation network in the permafrost regions of the Cryosphere Research Station on the QXP. Meteorological data were observation by automatic meteorological stations from a comprehensive observation network. The soil temperature and moisture data were collected from an integrated observation

https://doi.org/10.5194/essd-2021-1
Preprint. Discussion started: 8 February 2021

system in the active layer. Deep ground temperature was observed from boreholes. These datasets were helpful for the scientists with multiple study fields (i.e., climate, cryospheric, ecology and hydrology, meteorology science), which will greatly promote the verification, development and improvement of the hydrological model, land surface process model and climate model on the QXP. The datasets are available from the National Tibetan Plateau/Third Pole Environment Data Center (https://data.tpdc.ac.cn/en/disallow/789e838e-16ac-4539-bb7e-906217305a1d/, doi: 10.11888/Geocry.tpdc.271107).

1 Introduction

Permafrost is widely distributed on the QXP, which is called the "Third Pole of the Earth" (Qiu, 2008), is about 1.06×10^6km^2 in area and accounting for approximately a quarter of the QXP (Zou et al., 2017). Its unique and complicated hydrothermal process has great regulating effects on ground surface moisture, energy and mass exchange, ecosystem stability and carbon cycles (Cheng et al., 2019; Schuur et al., 2011). The surface energy and water cycle over the QXP have great influence on Asian monsoon, East Asian atmospheric circulation and global climate change (Ma et al., 2017; Yao et al., 2017). The characteristics of diabatic heating field of QXP are also used as an important factor for the short-term climate prediction in China (Liu and Hou, 1998; Wu et al., 2009; Ye and Gao, 1979).

The permafrost in the QXP has experienced significant degradation in response to climate warming, which mainly manifested as the permafrost area shrinking and ground temperature rise, the increased active layer, and decreased permafrost thickness (Hu et al., 2019b; Sharkhuu et al., 2007; Wang et al., 2000; Cheng et al., 2019). The permafrost degradation has caused the changes of surface vegetation characteristics. It was reported that the area of Alpine meadow on the QXP decreased by 16.2×10^4km^2 (accounted for 32.4% of the QXP (Zhao and Sheng, 2015)) in recent decades, which caused the change in hydrological processes, ecological environment and further led to desertification (Cheng and Jin, 2013; Cheng et al., 2019; Wu et al., 2003; Zhao et al., 2019). In addition, permafrost degradation could result in the decomposition of organic matter and greenhouse gases increased, which will finally affect the surface energy balance and the climate system (Wang et al., 2006a; Ping et al., 2015; Schuur et al., 2015; Schuur et al., 2011; Wu et al., 2012; Hu et al., 2019a). Permafrost degradation have also altered the geomorphological features and affected the stability of engineering structures in this region (Zhao et al., 2017).

https://doi.org/10.5194/essd-2021-1
Preprint. Discussion started: 8 February 2021

However, the collection of long-term and high resolution data over the permafrost regions of QXP is challenging due to the complex terrain, severe weather, and inconvenient to access (Ma et al., 2008; Li et al., 2012). Previous studies on the permafrost are focused on local and sites scale and major along the Qinghai-Tibet highway/Railway (Cuo et al., 2015; Su et al., 2013). Some new observation sites in permafrost regions in the vast western territory of the QXP were reported in recent years (Zhao et al., 2017; Zhao et al., 2018; Zhao et al., 2020). It is urgent to establish a synthesis observational database of permafrost thermal state and its climatic background to satisfy the requirements of calibration and validation for remote sensing interpretation and hydrothermal processes simulation, and also for the key parameters acquisition in permafrost regions (Bao et al., 2016; Li and Koike, 2003; Wang et al., 2017; Zhang et al., 2008; Hu et al., 2020). The complexity of the dynamic process of water and heat in freeze-thaw cycles is also considered to be one of the important reasons why the land surface model is not effective in simulating the permafrost change (Chen et al., 2014; Hu et al., 2016; Yang et al., 2018). Nevertheless, it is of great significance to provide a set data in thermal dynamic characteristics of the permafrost on the QXP (Wang et al., 2006b; Zhao et al., 2004).

The Cryosphere Research Station on the Qinghai–Xizang Plateau, Chinese Academy of Sciences (CRS-CAS), has established a comprehensive and widely permafrost monitoring network on the QXP (Zhao et al., 2019, 2020). This network is mainly focus on monitoring permafrost and its environmental factors in very high and cold regions of the QXP. Since the station was established in 1987, we have conducted long-term continuous monitoring and large-scale field investigations on permafrost of the QXP, and thus synthetically studied the mechanisms of the change in hydrothermal conditions of permafrost and their simulations and ecological effects. This paper first integrated air temperature, ground temperatures, soil moisture and permafrost temperature dataset over the permafrost regions across QXP from the CRS-CAS monitoring networks. The comprehensive permafrost monitoring network is summarized in Sect. 2. In Sect. 3, the datasets are described in detailed, with data evaluated and analysis. In Sect. 4, the data availability and access are provided, and in Sect. 5, the conclusions and future work are summarized.

2 Monitoring networks and data processing

2.1 Permafrost monitoring networks

https://doi.org/10.5194/essd-2021-1
Preprint. Discussion started: 8 February 2021

The thermal state of permafrost is mainly controlled by climate, and affected by land surface and geological conditions. The ecosystem in the permafrost region mainly dominated by alpine meadow, swamp meadow, alpine steppe, and alpine desert (Wang et al., 2016). The soils in the western permafrost region are Gelisols, Inceptisols and Aridisols, and in the eastern mainly consists of Gelisols, Mollisols and Inceptisols (Li et al., 2015). The permafrost monitoring network include 6 automatic meteorological stations, 8 active layer sites and, 77 boreholes (Fig. 1, Table 1). The elevation of all the sites are extremely high, exceeding 4000 m above the sea level (31.82~37.75 °N, 77.58~99.50 °E).

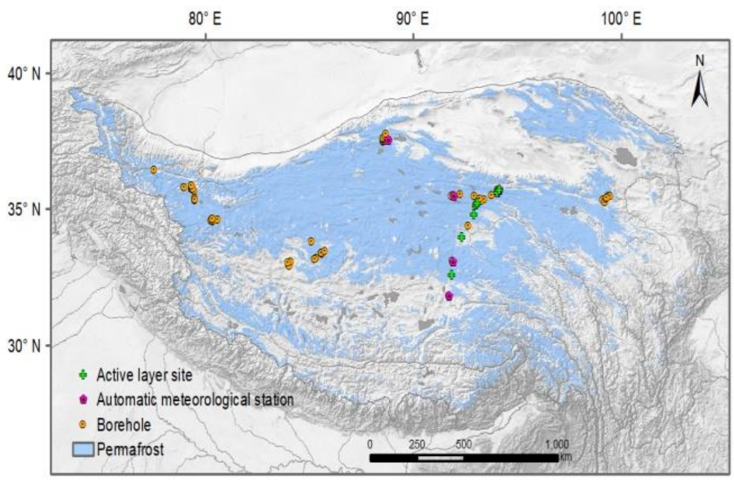

Figure 1. The permafrost monitoring networks on the QXP

There are only 4 national meteorological stations in the vast territory of permafrost regions. We set 6 automatic meteorological stations (Figure 2) within the permafrost zone gradually since 2004, the main observation indices include air temperature, humidity, wind speed gradient observation, radiation balance, and precipitation, etc. These six stations also include an active layer observation system and borehole monitoring simultaneously record frozen soil temperature, and are represent different permafrost, climate, vegetation, soil and other characteristics in different regions of the QXP. LDH has the lowest latitude, and it gets the warmest air temperature and the largest annual precipitation, while TSH and AYK which located in the northwest and north of the plateau, respectively, have the minimum and penultimate temperatures and annual precipitations. TSH has the highest solar radiation among the 6 stations.

https://doi.org/10.5194/essd-2021-1
Preprint. Discussion started: 8 February 2021

XDT and TGL are two sites with the longest sequence of 6 gradient meteorological stations. They were established in May 2004 and have had data accumulation over 16 years. XDT is located in the northern part of the QXP, near the northern permafrost boundary of the QXP. It represents the characteristics of the island-shaped permafrost area. TGL site is located on the north side of the Tanggula Mountains in the hinterland of the QXP and represents the characteristics of the continuous permafrost area. LDH is a new site established in 2014, is also located along the Qinghai-Tibet Highway. It is near the southern boundary of the permafrost region on the QXP, and can represent the characteristics of the discontinuous permafrost region. ZNH is located in the source of the Yangtze River, is an extremely rare observation station established in the vast unmanned area of the Qiangtang Regions of the QXP. It fills the data gap in the central and northern areas of the QXP and also located in a continuous permafrost area. AYK is located in the Altun Mountains area in the northern Tibetan Plateau, which is also a vast unmanned area as Qiangtang Region and is one of the areas with few observations. TSH is located in the West Kunlun Mountain area where is also an inaccessible area, is at the western border of the permafrost region on the QXP. It can reflect the regional characteristics of arid, cold, and high altitude in the western part of the QXP. The ground temperature and soil moisture observed of active layer and permafrost was summarized in Table 1.

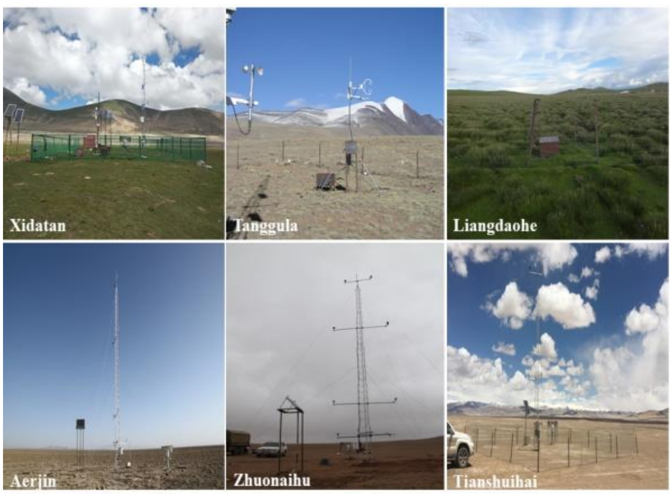

Figure 2. The six comprehensive meteorological stations

Table 1 The observation instruments and items for meteorological data, ground temperature and soil water content

Observation site type	Available sites	Observation item	Instrument	Accuracy	Height/Depth

Meteorological Stations	6	Upward/downward short-wave radiation	CM3, Kipp & Zonen, Holland	±10%	2 m
		Upward/downward long-wave radiation	CM3, Kipp & Zonen, Holland	±10%	2 m
		Air temperature	HMP45C, Vaisala Finland	±0.5 ℃	2，5，10 m
		Air humidity		±3% RH	2，5，10 m
		Wind velocity	05103_L/RM, Campbell, USA	±0.3 m/s	2，5，10 m
		Precipitation	T-200B Precipitation Gauge	±0.1 mm	5 m away
Active Layer	10	Soil temperature	105T/109 Thermocouple temperature sensor	±0.1 ℃ ±0.2 ℃	0.5 m,1.0 m,2 m, >2 m
		Soil moisture content	CS616/ Hydra Soil moisture sensor	±2.5%	
Borehole	40	Ground Temperature	Thermistor, SKLFSE, CHINA	±0.05 ℃	0.4 m - 34.5 m (total 47 layers)

2 Monitoring data

The main observation items and instruments for the meteorological observations were shown in Table 1. The observation was done every 10 minutes, and was averaged and recorded every 30 minutes automatically. The data were recorded by CR10X, CR1000 and CR3000 data logger (Campbell Scientific). Meteorological data (e.g., the precipitation, radiation, air temperature, relative humidity and wind speed) were recorded hourly with a CR1000/CR3000 data acquisition instrument (Campbell Scientific Inc., USA) (Fig 3a). There were three measured at heights of 2 m, 5 m and 10 m for air temperature, relative humidity and wind speed (Table 3).

https://doi.org/10.5194/essd-2021-1
Preprint. Discussion started: 8 February 2021

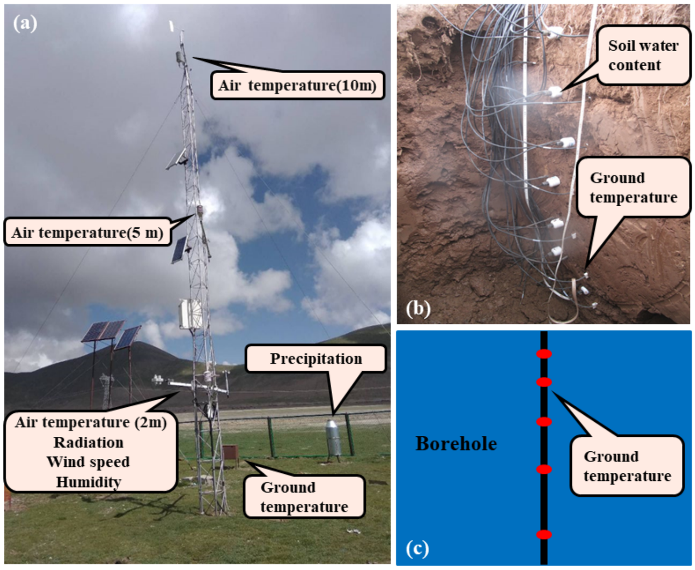

Figure 3. The comprehensive observation system : (a) meteorological observation, (b) ground temperature and soil water content in the active layer and (c) ground temperature observation for permafrost.

The ground temperature was measured at different depths from ground surface to the depth of 10 to 50 cm below the permafrost table with a 105T/109 thermocouple Probe with an accuracy of ± 0.1 ℃/± 0.2 ℃ in the active layer (Fig 3b). The soil water content was measured by a Hydra soil moisture sensor (Table 1), by connecting to a CR10X/CR1000/CR3000 data logger (Campbell Company, USA).

The ground temperature in the borehole was measured by the Thermistors (with an accuracy of ± 0.1 ℃) produced by the State Key Laboratory of Frozen Soil Engineering, Cold and Arid Regions Environmental and Engineering Research Institute of the Chinese Academy of Sciences (SKLFSE, CAREERI, CAS), which were installed in the boreholes and connected to an automatic data logger (CR1000/ CR3000, Campbell Scientific Company, Logan, UT, USA) to monitor ground temperatures at various deep depths (Table 1) (Fig 3c).

2.3 Data processing workflow

Data processing workflow is showed in Figure 4. All data are under quality control before processing. The quality control was two-fold: (1) the missing data were replaced by -6999; (2) the singular unphysical data were rejected, and the gaps were replaced by -6999. In addition, all the

https://doi.org/10.5194/essd-2021-1
Preprint. Discussion started: 8 February 2021

Open Access Earth System Science Data Discussions

daily data were calculated by every 30 min (1 h) interval per day. The active layer thickness was derived by the maximum depth of 0 ℃ isotherm from linear interpolation of the daily maximum ground temperature. The monthly means air and ground temperatures, radiation, wind speed, relative humidity and soil water content were also calculated. The dataset also provides mean-annual air temperature (MAAT); mean-annual ground temperature at depth of 0.5 m, 0.75 m, 1.0 m, 1.5 m, 2 m and >2 m; and maximum and minimum ground temperature. The trend of air temperature, active layer thickness, and ground temperature is analyzed and provided at the stations with long time observation.

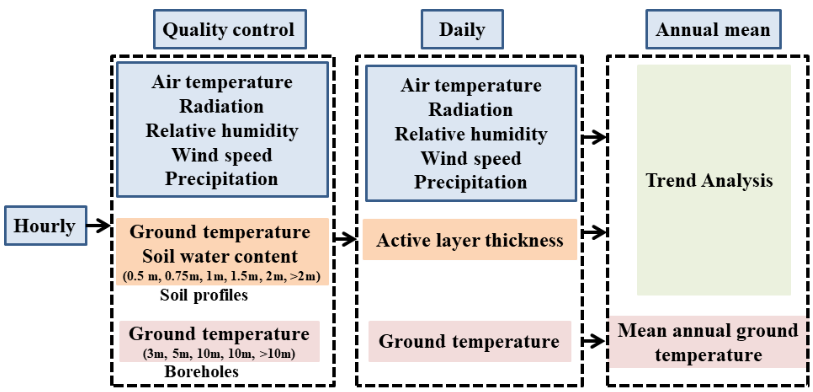

Figure 4. Schematic diagram of data processing workflow used to compile the permafrost dataset on the QXP.

3 Data description and evaluation

3.1 Meteorological data

Table 2. The information of six meteorological stations

Sites	XDT	TGL	LDH	ZNH	AYK	TSH
Latitude (ºN)	35.72	33.07	31.82	35.49	37.54	35.62
Longitude (ºE)	94.13	91.94	91.74	91.96	88.8	94.06
Elevation (masl)	4538	5100	4808	4784	4300	4844
Vegetation	Alpine steppe	Alpine meadow	Alpine wet meadow	Alpine desert	Alpine desert	Alpine desert steppe

https://doi.org/10.5194/essd-2021-1
Preprint. Discussion started: 8 February 2021

Observation height above the ground surface (m)	2,5,10	2,5,10	2,5,8	2,4,10,15	2,4,10,15	2,4,10
Data since	2004.5	2004.5	2014.9	2013	2013	2015
Missing date	17.7~17.9	09.6~09.8, 16.10~17.9, 17.12~18.1,	18.1~18.4	14.7~15.4 (Ta, Preci.)	15.8~15.9	Ws at 2m
Ta (°C)	-3.6	-4.7	-2.3	-4.9	-5.2	-6.0
RH (%)	53.5	51.5	48.2	53.9	46.1	40.6
Precipitation (mm)	384.5	352.0	388.6	277.8	158.6	103.3
Wind speed (m/s)	4.1	4.1	3.2	4.7	4.5	
DSR (W/m^2)	224.2	233.4	231.4	204.8	198.2	250.8
USR (W/m^2)	66.8	61.4	46.6	46.3	53.8	68.5
DLR (W/m^2)	223.0	214.8	237.2	233.8	223.0	211.5
ULR (W/m^2)	304.5	304.5	315.9	303.2	307.6	311.3
Net radiation	75.9	82.3	106.0	89.2	59.8	82.5

The mean annual air temperatures (MAAT) of all 6 sites are between -2.3 ~ -6 °C, and their seasonal variation are significant (Fig. 5). The mean monthly air temperatures in 3 seasons except summer are lower than 0 °C. The difference of the air temperatures between these stations were mainly caused by the difference in altitude and latitude. Although the difference in summer is relatively small, it is very large in winter, and is obvious in spring and autumn.

Precipitation shows significant seasonal variation, which is closely related to the monsoon cycles. The precipitation from May to September is more than 85% of its annual amounts at the sites other than TSH (78.6%). Most of the precipitation is concentrated in summer. A small amount is in late spring and early autumn, and rare in the winter. Precipitation has significant spatial difference, which is more than 350 mm in average at XDT, TGL, LDH along the Qinghai-Xizang Highway, and is relatively higher than other sites in the western QXP. The precipitation at ZNH, located in the hinterland of the plateau, is slightly lower, and is about 150 mm (slightly higher than

https://doi.org/10.5194/essd-2021-1
Preprint. Discussion started: 8 February 2021

half at ZNH) in AYK and much lower, which is located on the northern edge of the Tibetan Plateau and has the highest latitude among all the 6 sites. The annual total precipitation at TSH is the lowest of all the observation sites, and is only 100 mm, which is located near the western boundary of QXP.

The air humidity exhibits seasonal variation, which are very consistent with the change of air temperature and precipitation. The difference between the stations is related to the precipitation, especially in summer. Due to the scarce precipitation, the relative humidity at TSH is at a low level throughout the year. And it is similar in AYK. It is worth noting that the relative humidity in TGL and LDH is quite low in winter. Since their latitude are lower, the air temperatures in winter are higher. The ground evaporates more and becomes drier. The wind speeds at all stations on the plateau are generally high. Except LDH, the average annual wind speeds are all above 4 m/s. The wind speed is the highest in winter, followed by spring and the lowest in summer. The wind speed of LDH shows a low state throughout the year, due to its latitude and local conditions. It is located in a well-developed swamp meadow area with a gentle slope, where the vegetation is lush.

Downward shortwave radiation (total solar radiation) usually reaches its maximum in May, at most sites except TSH. This is due to the concentration of rain in summer. Therefore, the mean downward shortwave radiation in summer is only slightly higher than that in spring. However, at TSH (with little precipitation), it is very high in summer, and also significantly higher than other sites in spring and autumn. The upward shortwave radiation is mainly restricted by the surface albedo. Its high value is mainly affected by the snow on the ground. Its seasonal changes reflect that the snow cover may mainly appear in autumn, followed by spring and relatively little in winter. The upward short-wave radiation of TSH in all seasons is high, which is related to the area with less precipitation and the surface is almost dry and bare. The upward and downward long-wave radiation is closely related to air temperature and surface temperature, respectively, and their seasonal variation trend is basically consistent with the change of air temperature.

https://doi.org/10.5194/essd-2021-1
Preprint. Discussion started: 8 February 2021

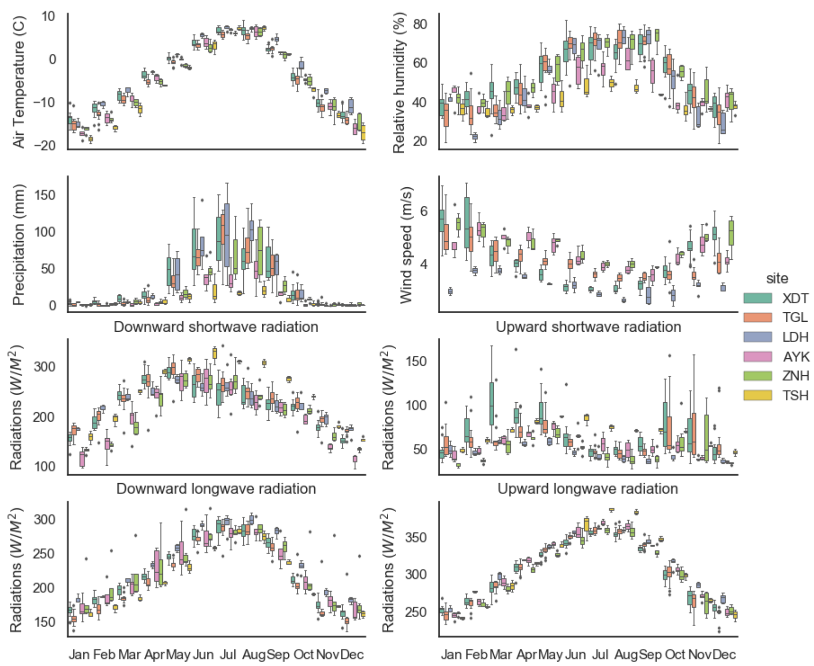

Figure 5. Characteristics of monthly observation variables at six meteorological stations

XDT and TGL stations can provide basic data for physical process research and land surface process model research. The annual mean temperature of the two stations showed increasing trends, with rates of 0.66 and 0.40 °C/10a, and p-values of 0.27 and 0.23, respectively. The warming trend is the highest in summer and autumn, and has a good significance. However, the temperature in winter shows a weak decrease. The precipitations show an insignificant week decrease trend (-15.0 and -14.3 mm/10a). It shows a slightly decreasing trend in summer and autumn, and an increasing trend in spring (Fig. 6).

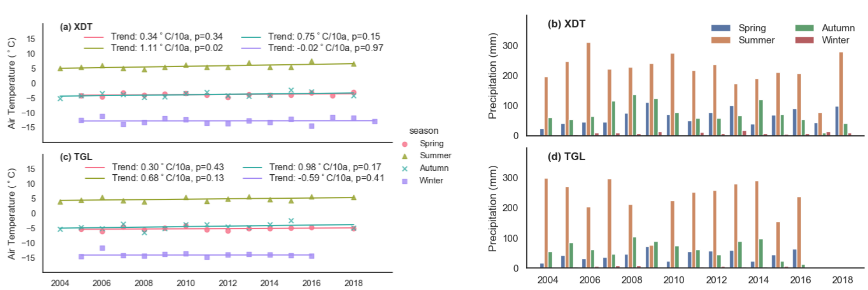

https://doi.org/10.5194/essd-2021-1
Preprint. Discussion started: 8 February 2021

Figure 6. Seasonal mean series and changes of temperature and precipitation at XDT and TGL from 2004 to 2018

3.2 Active layer thickness

The active layer thicknesses varied from about 120 cm to about 300 cm along Qinghai-Tibet highway under different surface vegetation conditions (Fig.7). Ch04, which locates at sporadic island permafrost of the QTB southern permafrost distribution limit regions under swamp meadow condition, appeared as the shallowest active layer site. Its average thickness was 116 cm during years of 2000-2018. The deepest active layer appeared at QT05, which locates at the margin of permafrost from taliks formed by the thermal influences from the tributaries of Yangtze River headwaters, Tongtian river and Tuotuo river. Its average thickness was 307 cm from 2004 to 2013, where the surface vegetation is alpine meadow. In the continuous permafrost zone of QXP, which include Ch06, QT08, QT01, QT03, and Ch01 sites, the shallowest active layer located at the Kunlun Mountains pass (Ch06) under nearly bare land surface vegetation condition. Its average thickness was 147 cm during years of 2005-2018. The deepest active layer located at Wudaoliang (QT08) under bare land. Its average thickness was 235 cm during years of 2010-2018. For representative alpine meadow conditions, for example QT01 at Wudaoliang and Ch01 at Fenghuo Mountains, their average thicknesses were 163 cm and 167 cm. While at Beiluhe (QT03), about 10 km north of Ch01 site, its average thickness was about 231 cm with typical alpine meadow condition, which is apparently larger than QT01 and Ch01. In addition, the QT09 locates at the north limit permafrost distribution region, named Xidatan. Its average active layer thickness was 141 cm during years of 2011-2018 under typical alpine meadow condition. On the whole, in our opinion, the ground surface vegetation conditions may have some influences on active layer thickness spatial distribution. But it is not a control factors, especially at large spatial scale. The spatial distribution of active layer thickness was jointly influenced by climate conditions, ground temperature (including ground surface temperature and permafrost layer temperature), soil water content, soil texture. Due to the great spatial variation of these above influencing factors, the active layer thickness within our monitoring regions presented as great spatial variation.

In terms of time variation, all the monitoring sites showed the same pattern. Their active layer thicknesses were increasing gradually. But their increasing rate were very different amount sites,

https://doi.org/10.5194/essd-2021-1
Preprint. Discussion started: 8 February 2021

with the largest increasing rate of 3.9 cm/yr at Ch01 and the lowest increasing rate of 0.8 cm/yr at QT05. Of which worth noting is that the active layer thickness increasing rate is very sensitive to the statistical period. Taking QT09 for example, its average increasing rate was 3.0 cm/yr during 2011-2018. While during years of 2014-2018, its average increasing rate was 6.9 cm/yr. So the statistical active layer thickness increasing rates can't be considered as a long term thickness increasing trend. It only revealed that the active layer thickness has a slow increase trend with inter-annual fluctuation, and their increasing amplitudes are very different amount different monitoring sites.

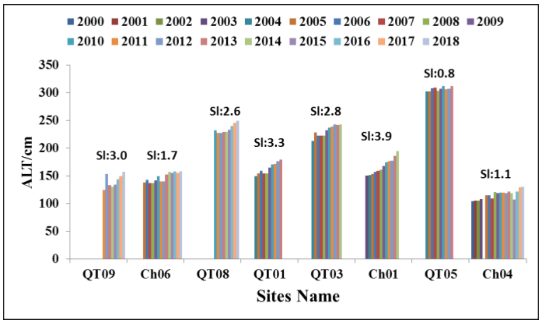

Figure 7. Variation in active layer thickness among different sites. SI represents the active layer thickness average annual increasing rate.

3.3 Ground temperature

3.3.1 Temperature in the active layer

In this section, we choose ground temperature at 10cm depth and at the base of active layer of years 2011-2013, during which all eight active layer monitoring sites had continuous ground temperature monitoring data series, to analyze the active layer ground temperature spatial distribution and their influence on active layer thickness spatial distribution (Table.5). The ground temperature (ALT_Base_GT) was derived from geothermal interpolation when there was no temperature probe at the real active layer depth position at the base of active layer. For all 8 active layer monitoring sites, the mean annual ground temperature (10cm_GT) varied greatly from site to site at 10cm depth. The lowest 10cm_GT appeared at Kunlun Mountains region (Ch06),which is -2.86℃. For QT03, QT05 and Ch04, the 10cm_GT were positive, and as high as 1.12℃ and 1.25℃ at sites QT05 and Ch04. For ALT_Base_GT, the relative low temperature all appeared at mountain

https://doi.org/10.5194/essd-2021-1
Preprint. Discussion started: 8 February 2021

regions, such as Ch06 at Kunlun Mountains and Ch01 at Fenghuo Mountains. This because the ALT_Base_GT was simultaneously influenced by ground surface temperature and underlain permafrost temperature, and in mountains regions, the permafrost layer temperature is often very low in QXP. At the marginal regions of permafrost distribution or island permafrost region, such as QT09, QT05 and Ch04, the ALT_Base_GT were relatively higher than other sites due to their high underlain permafrost layer temperature.

Table. 3 The mean active layer thickness, ground temperature at depth of 10 cm and permafrost table

Sites Name	ALT/cm	10cm_GT/℃	ALT_Base_GT/℃
QT09	137	-1.3	-1.34
Ch06	146	-2.86	-2.68
QT08	228	-1.64	-1.45
QT01	176	-1	-1.7
QT03	241	0.03	-1.29
Ch01	180	-1.35	-2.47
QT05	308	1.12	-0.17
Ch04	120	1.25	-0.51

The scatter plot between active layer thickness and 10 cm_GT showed that, on the whole, ALT increased with the increasing of 10 cm_GT, but they are not linear dependent (Fig.8). Especially for Ch04 at island permafrost region under swamp meadow surface vegetation, the relationship between ALT and 10 cm_GT was very different from other monitoring sites. This demonstrates that surface ground temperature spatial distribution did have influence on ALT distribution, but it can’t be used as a main control factor for ALT prediction under different soil and vegetation conditions. Contrast to the relationship between ALT and 10cm_GT, the relationship between ALT and ALT_Base_GT is much better (Fig.3.2-2 b). If without considering the large deviation of sites QT09 and Ch04, active layer thickness was nearly linear dependent on the variation of ALT_Base_GT, which indirectly showed that the underlain permafrost temperature properties have great influence on ALT distribution.

https://doi.org/10.5194/essd-2021-1
Preprint. Discussion started: 8 February 2021

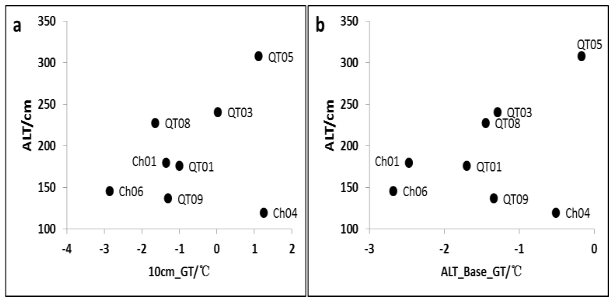

Figure 8. The relationship between active layer thickness and the temperature of permafrost table

In the dataset, the shallow ground temperature of 8 active-layer monitoring sites were collected with automatic data logger along the Qinghai-Tibetan Road. At these sites, the annual mean ground temperature at 10cm ranged from -2.62 ℃ to -0.20 ℃, while the mean temperature near top of permafrost ranged from -2.69 ℃ to -0.37 ℃. The temperature at two depths has a good linear correlation. The mean ground temperatures near the top of permafrost at 6 sites were 0.30 ℃ to 1.83 ℃ lower than the temperature of 10 cm. At only 2 sites (CN06 and QT08), the former is slightly higher than the latter (approximately 0.2 ℃). The subsurface ground temperature of 10cm at all the sites showed increasing trends with increase rates ranging from 0.03 to 0.19 ℃ per year, and the maximum rate occurred at site QT09 which locates the northern marginal region of permafrost. The increasing rate at the bottom of the active layer (near top of permafrost) is slightly lower than rate of surface active layer. Even at CN06, there was a slight cooling trend at the bottom of the active layer.

3.3.2 Ground temperature from boreholes

Fifteen borehole sites automatically collected ground temperature at different depths; 14 of them located in the permafrost regions and only one is located in a structural talik region (QTB11).

Annual mean ground temperatures at depth of 3 m and 6 m are listed in Table L1. The ground temperature of these two horizons at most sites not only has obvious seasonal variation, but also has remarkable inter-annual variation. Except for QTB11 that locates in the seasonal frozen ground region, the available mean annual ground temperatures at 10m and 20m are respectively shown in the Figure 10. For the temperature of 10 m, the highest permafrost temperature appears at site QTB05 that locates in Qumar River along the Qinghai-Tibetan Road, the mean annual ground temperature of which is very close to 0 ℃, and meanwhile the active layer thickness has

https://doi.org/10.5194/essd-2021-1
Preprint. Discussion started: 8 February 2021

approximately exceeded 9 m. The lowest temperature appears at site FCKGT that locates in high plain area in the south of the Altun Mountain, where the permafrost temperature reaches -4 °C due to extremely cold and dry climatic conditions. The ground temperature at all 15 boreholes showed significant linear increasing trends, and the permafrost has warmed at different rates. The warming rates at depth of 10m ranged from 0.02 °Cper decade (FCKGT) to 0.78 °C per decade (QTB05), but increasing rates of temperature at depth of 20m were much smaller than 10 m, and varied between 0 °C per decade and 0.24 °C per decade. The annual mean temperature of 20 m at site ZNHGT has rarely changed during the period from 2013 to 2018. At this depth, the most significant warming occurred at site QTB02, QTB18 and QTB15. The warming rate of permafrost seems to have a strong relationship with the temperature of permafrost itself.

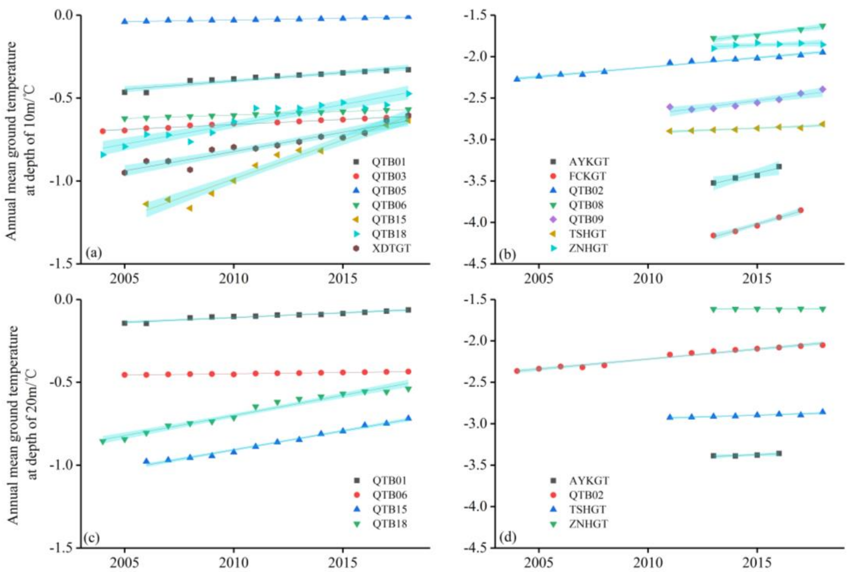

Figure 9. Annual mean ground temperature as a function of time at depth of 10m(a, b) and 20m(c, d) from borehole with continuous data series

Figure 10a shows that the change rate of ground temperature at two shallow depths (10 cm and the depth near top of permafrost). They show a trend of increasing first and then decreasing as the temperature near the bottom of the active layer rises. Both colder and warmer sites have relatively smaller variation rate of ground temperature. The sites with ground temperature between -2 °C and -1 °C have the greatest ground warming rate. However, the deep ground temperature shows another

https://doi.org/10.5194/essd-2021-1
Preprint. Discussion started: 8 February 2021

pattern and lower temperature permafrost tend to have a great warming rate (Figure 10b). It is consistent with previous research results at Qinghai-Tibetan Plateau, and the correlation between permafrost temperatures and warming rates is more significant. It indicates that the ice-water phase transition effect in the conversion from permafrost to melting soil has significantly slowed the process of ground temperature increase.

We also analyzed another 62 sites of which the ground temperatures are recorded manually. The altitude of these sites ranges from 4142 to5247 m a.s.l. The drilling depth of borehole reached 10m at most of the sites, several reach 20m. The observation interval is once every one year or two years., the multi-year averages based on single observations are calculated to compare the thermal regime of different sites (Table L2). The multi-year mean ground temperature of 10m observed at different sites ranged from -3.84 °C to 3.36 °C. There are 10 observation fields with a positive mean ground temperatures of 10 m and 52 fields with negative values. The site with highest ground temperature is HT01, and the one with lowest temperature is STG. For all observation sites, the ground temperature shows a slightly downward trend as the elevation increases.

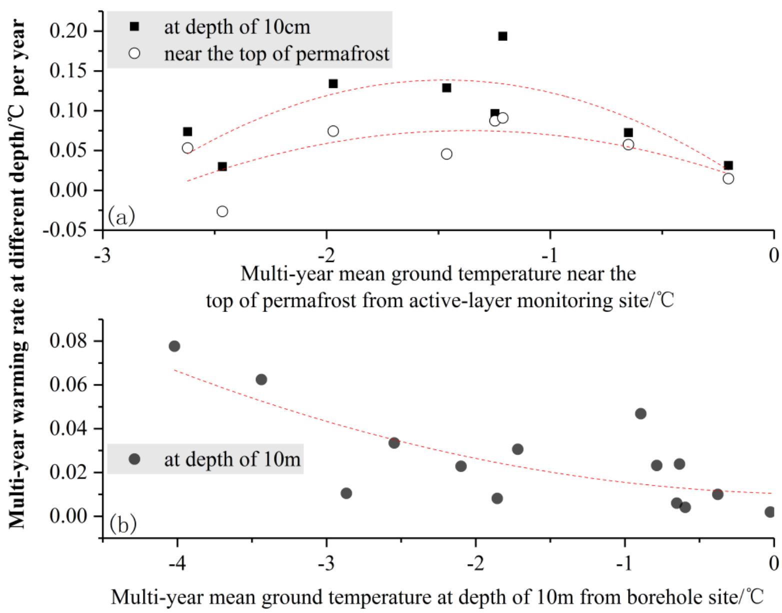

Figure 10. The relationship between warming rate and multi-year mean ground temperature during observation period from active-layer monitoring site (a) and borehole site (b).

https://doi.org/10.5194/essd-2021-1
Preprint. Discussion started: 8 February 2021

3.3 Soil moisture

The average volumetric soil water content (VWC) within ALT were calculated with depth-weighted average method at time of ground surface begin to freeze and ALT reached its max thawing depth at each monitoring sites (Fig.11a). In terms of inter-annual change, VWC had no obvious changing trend with random inter-annual fluctuations. In terms of spatial variation, the VWC varied from 0.141 to 0.403 m^3/m^3 among our monitoring sites, with the largest VWC at Ch04 and the lowest at QT08. Active layer soil water content was basically controlled by ground surface vegetation conditions, soil texture and local drainage conditions. For example, it was swamp meadow at Ch04 with about 60 cm depth of peat soil layer beneath ground surface. This resulted in the very shallow active layer thickness and nearly saturated soil water content condition. At QT05, the soil pit excavated in 2007 revealed that it was sand within 140 cm. This site has very bad drainage condition and resulted in relatively high VWC, averaged 0.292 m^3/m^3 during 2004-2018. While at QT08, where the soil type is also sand within active layer, because of its very good drainage condition, VWC is very low, averaged 0.141 during 2012-2018.

Converting the VWC into total soil water depth per unit area that stored within active layer, soil water depth varied from 290 mm to 890 mm among our monitoring sites (Fig.11b). QT05 had the highest soil water depth, averaged 890 mm during 2004-2008. High soil water depth must absorb high heat energy during active layer thawing process. This can explain why the active layer thickness increasing rate was very low, while its ground surface temperature was very high.

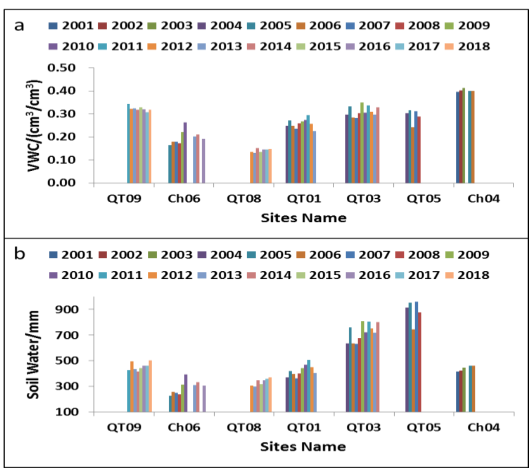

Figure 11. Variation in volumetric water content and soil water equivalent among different sites

4 Data availability

All datasets in this paper have been released and can be free download from the National Tibetan Plateau/Third Pole Environment Data Center (https://data.tpdc.ac.cn/en/disallow/789e838e-16ac-4539-bb7e-906217305a1d/,doi: 10.11888/Geocry.tpdc.271107) or Cryosphere Research Station on Qinghai-Xizang Plateau (http://new.crs.ac.cn/).

5 Conclusions

The observation data in permafrost regions on the QXP can provide basic data for the study of land-atmosphere interaction and climate change research. They could provide accurate inputs and verifications data for land surface models, reanalysis data and remote-sensing products, and climate models. The results revealed that the annual mean air temperatures of all 6 sites are between -2.3 ~ -6 ^{o}C, and their seasonal variation characteristics are significant. Precipitation shows a significant seasonal change trend, which is closely related to the monsoon period. The annual mean air temperature of the XDT and TGL stations showed increasing trends, with rates of 0.66 and 0.40 ^{o}C/10a, respectively, and ground temperature has significant warming trend. The precipitations show an insignificant week decrease trend. The active layer thickness has a slow increase trend with inter-annual fluctuation, and their increasing amplitudes are very different amount different monitoring sites. In addition, from the high-quality comprehensive dataset with a focus on permafrost thermal state on the QXP, which could provide accurate and effective forcing data and evaluation data for different models. This valuable permafrost dataset is worth maintaining and promoting in the future due to hard-won. It also provides a prototype of basic data collection and management for other permafrost regions.

Author contributions. L Zhao generated and designed the observation network, participated the field installation of most of the observations sites, found supports for maintaining the observation systems. DF Zou, GJ Hu, TH Wu, XD Wu, R Li, EJ Du, GY Liu, YP Qiao and X Yao participated the field works and maintained the observation sites. GJ Hu, R Li, EJ Du, GY Liu, X Yao and DF Zou performed data processing, organization and analyses. GJ Hu, L Zhao, EJ Du, GY Liu, X Yao and DF Zou wrote the paper, and all authors participated the manuscripts revision.

Competing interests. No conflict of interest.

Acknowledgements. We would like to thank all the scientists, engineers, and students who participated in the field work and maintain this observation network and data acquisition.

Financial support. This work was financially supported by the National Natural Science Foundation of China (41931180), the Second Tibetan Plateau Scientific Expedition and Research (STEP) program, China (2019QZKK0201), and the National Natural Science Foundation of China (42071094, 41701073).

Reference:

Bao, H., Koike, T., Yang, K., Wang, L., Shrestha, M., and Lawford, P.: Development of an enthalpy-based frozen soil model and its validation in a cold region in China, J. Geophys. Res.-Atmos., 121, 5259-5280, https://doi.org/10.1002/2015jd024451, 2016.

Chen, B., Luo, S., Lu, S., Zhang, Y., and Ma, D.: Effects of the soil freeze-thaw process on the regional climate of the Qinghai-Tibet Plateau, Climate Research, 59, 243-257, https://doi.org/10.3354/cr01217, 2014.

Cheng, G., and Jin, H.: Groundwater in the permafrost regions on the Qinghai-Tibet Plateau and it changes, Hydrogeology & Engineering Geology, 40, 1-11, 2013.

Cheng, G., Zhao, L., Li, R., Wu, X., Sheng, Y., Hu, G., Zou, D., Jin, H., Li, X., and Wu, Q.: Characteristic, changes and impacts of permafrost on Qinghai-Tibet Plateau, Chinese Science Bulletin, 64, 2783-2795, 2019.

Cuo, L., Zhang, Y., Bohn, T. J., Zhao, L., Li, J., Liu, Q., and Zhou, B.: Frozen soil degradation and its effects on surface hydrology in the northern Tibetan Plateau, Journal of Geophysical Research: Atmospheres, 120, 8276-8298, https://doi.org/10.1002/2015JD023193, 2015.

Hu, G., Zhao, L., Wu, X., Li, R., Wu, T., Xie, C., Qiao, Y., Shi, J., Li, W., and Cheng, G.: New Fourier-series-based analytical solution to the conduction-convection equation to calculate soil temperature, determine soil thermal properties, or estimate water flux, International Journal of Heat and Mass Transfer, 95, 815-823, https://doi.org/10.1016/j.ijheatmasstransfer.2015.11.078, 2016.

Hu, G., Zhao, L., Li A, R., Wu, X., Wu, T., Zhu, X., Pang, Q., Liu, G. Y., Du, E., Zou, D., Hao, J., and Li, W.: Simulation of land surface heat fluxes in permafrost regions on the Qinghai-Tibetan Plateau using CMIP5 models, Atmospheric Research, 220, 155-168, https://doi.org/10.1016/j.atmosres.2019.01.006, 2019a.

Hu, G., Zhao, L., Wu, X., Wu, T., Li, R., Xie, C., Xiao, Y., Pang, Q., Liu, G., Hao, J., Shi, J., and Qiao, Y.: Variations in soil temperature from 1980 to 2015 in permafrost regions on the Qinghai-Tibetan Plateau based on observed and reanalysis products, Geoderma, 337, 893-905, https://doi.org/10.1016/j.geoderma.2017.07.017, 2019b.

Hu, G., Zhao, L., Zhu, X., Wu, X., Wu, T., Li, R., Xie, C., and Hao, J.: Review of algorithms and parameterizations to determine unfrozen water content in frozen soil, Geoderma, 368, 114277, https://doi.org/10.1016/j.geoderma.2020.114277, 2020.

Li, R., Zhao, L., Ding, Y., Wu, T., Xiao, Y., Du, E., Liu, G., and Qiao, Y.: Temporal and spatial variations of the active layer along the Qinghai-Tibet Highway in a permafrost region, Chinese Science Bulletin, 57, 4609-4616, https://doi.org/10.1007/s11434-012-5323-8, 2012.

Li, X., and Koike, T.: Frozen soil parameterization in SiB2 and its validation with GAME-Tibet

observations, Cold Regions Science and Technology, 36, 165-182, https://doi.org/10.1016/s0165-232x(03)00009-0, 2003.
Liu, X., and Hou, P.: Relationship between the climatic warming over the Qinghai -Xizang Plateau and its surrounding areas in recent 30 years and the elevation, Plateau Meteorology, 17, 245-245, 1998.
Ma, L., Zhang, T., Li, Q., Frauenfeld, O. W., and Qin, D.: Evaluation of ERA-40, NCEP-1, and NCEP-2 reanalysis air temperatures with ground-based measurements in China, J. Geophys. Res.-Atmos., 113, https://doi.org/10.1029/2007jd009549, 2008.
Ma, Y., Ma, W., Zhong, L., Hu, Z., Li, M., Zhu, Z., Han, C., Wang, B., and Liu, X.: Monitoring and Modeling the Tibetan Plateau's climate system and its impact on East Asia, Scientific Reports, 7, https://doi.org/10.1038/srep44574, 2017.
Ping, C., Jastrow, J., Jorgenson, M., Michaelson, G., and Shur, Y.: Permafrost soils and carbon cycling, Soil, 1, 147-171, https://doi.org/10.5194/soil-1-147-2015, 2015.
Qiu, J.: The third pole, Nature, 454, 393-396, https://doi.org/10.1038/454393a, 2008.
Schuur, E., McGuire, A., Schädel, C., Grosse, G., Harden, J., Hayes, D., Hugelius, G., Koven, C., Kuhry, P., and Lawrence, D.: Climate change and the permafrost carbon feedback, Nature, 520, 171-179, https://doi.org/10.1038/nature14338, 2015.
Schuur, E. A. G., Abbott, B., and Permafrost Carbon, N.: High risk of permafrost thaw, Nature, 480, 32-33, https://doi.org/10.1038/480032a, 2011.
Sharkhuu, A., Sharkhuu, N., Etzelmüller, B., Heggem, E. S. F., Nelson, F. E., Shiklomanov, N. I., Goulden, C. E., and Brown, J.: Permafrost monitoring in the Hovsgol mountain region, Mongolia, Journal of Geophysical Research Atmospheres, 112, 195-225, https://doi.org/10.1029/2006JF000543, 2007.
Su, F., Duan, X., Chen, D., Hao, Z., and Cuo, L.: Evaluation of the Global Climate Models in the CMIP5 over the Tibetan Plateau, Journal of Climate, 26, 3187-3208, https://doi.org/10.1175/JCLI-D-12-00321.1, 2013.
Wang, G., Li, Y., Wu, Q., and Wang, Y.: Impacts of permafrost changes on alpine ecosystem in Qinghai-Tibet Plateau, Science in China Series D: Earth Sciences, 49, 1156-1169, 2006a.
Wang, G., Li, Y., Wu, Q., and Wang, Y.: Impacts of permafrost changes on alpine ecosystem in Qinghai-Tibet Plateau, Science in China Series D-Earth Sciences, 49, 1156-1169, https://doi.org/10.1007/s11430-006-1156-0, 2006b.
Wang, L., Zhou, J., Qi, J., Sun, L., Yang, K., Tian, L., Lin, Y., Liu, W., Shrestha, M., Xue, Y., Koike, T., Ma, Y., Li, X., Chen, Y., Chen, D., Piao, S., and Lu, H.: Development of a land surface model with coupled snow and frozen soil physics, Water Resour. Res., 53, 5085-5103, https://doi.org/10.1002/2017wr020451, 2017.
Wang, S. L., Jin, H. J., Li, S. X., and Zhao, L.: Permafrost degradation on the Qinghai-Tibet Plateau and its environmental impacts, Permafrost and Periglacial Processes, 11, 43-53, 2000.
Wu, B., Yang, K., and Zhang, R.: Eurasian snow cover variability and its association with summer rainfall in China, Advances in Atmospheric Sciences, 26, 31-44, 2009.
Wu, Q., Shen, Y., and Shi, B.: The relationship between frozen soil together with its water-heat process and ecological environment in the Tibetan Plateau, Journal of Glaciology and Geocryology, 25, 250-255, 2003.
Wu, X., Zhao, L., Chen, M., Fang, H., Yue, G., Chen, J., Pang, Q., Wang, Z., and Ding, Y.: Soil Organic Carbon and Its Relationship to Vegetation Communities and Soil Properties in Permafrost Areas of the Central Western Qinghai-Tibet Plateau, China, Permafrost and Periglacial Processes, 23, 162-169,

https://doi.org/10.1002/ppp.1740, 2012.

Yang, K., Wang, C., and Li, S.: Improved Simulation of Frozen-Thawing Process in Land Surface Model (CLM4.5), J. Geophys. Res.-Atmos., 123, 13238-13258, https://doi.org/10.1029/2017jd028260, 2018.

Yao, T., Piao, S., Shen, M., Gao, J., Yang, W., Zhang, G., Lei, Y., Gao, Y., Zhu, L., Xu, B., Yu, W., and Li, S.: Chained Impacts on Modern Environment of Interaction between Westerlies and Indian Monsoon on Tibetan Plateau, Bulletin of the Chinese Academy of Sciences, 32, 976-984, 2017.

Ye, D., and Gao, Y.: The Meteorology of the Qinghai-Xizang (Tibet) Plateau, Science Press: Beijing, 278 pp., 1979.

Zhang, Y., Carey, S. K., and Quinton, W. L.: Evaluation of the algorithms and parameterizations for ground thawing and freezing simulation in permafrost regions, J. Geophys. Res.-Atmos., 113, https://doi.org/10.1029/2007jd009343, 2008.

Zhao, L., Ping, C.-L., Yang, D., Cheng, G., Ding, Y., and Liu, S.: Changes of climate and seasonally frozen ground over the past 30 years in Qinghai–Xizang (Tibetan) Plateau, China, Global and Planetary Change, 43, 19-31, https://doi.org/10.1016/j.gloplacha.2004.02.003, 2004.

Zhao, L., and Sheng, Y.: Permafrost survey manual, Science Press: Beijing, 13-14 pp., 2015.

Zhao, L., Wu, T., Xie, C., Li, R., Wu, X., Yao, J., Yue, G., and Xiao, Y.: Support Geoscience Research, Environmental Management, and Engineering Construction with Investigation and Monitoring on Permafrost in the Qinghai-Tibet Plateau, China, Bulletin of the Chinese Academy of Sciences, 32, 1159-1168, 2017.

Zhao, L., Wu, X., Wang, Z., Sheng, Y., Fang, H., Zhao, Y., Hu, G., Li, W., Pang, Q., Shi, J., Mo, B., Wang, Q., Ruan, X., Li, X., and Ding, Y.: Soil organic carbon and total nitrogen pools in permafrost zones of the Qinghai-Tibetan Plateau, Scientific Reports, 8, https://doi.org/10.1038/s41598-018-22024-2, 2018.

Zhao, L., Hu, G., Zou, D., Wu, X., Ma, L., Sun, Z., Yuan, L., Zhou, H., and Liu, S.: Permafrost Changes and Its Effects on Hydrological Processes on Qinghai-Tibet Plateau, Bulletin of the Chinese Academy of Sciences, 34, 1233-1246, 2019.

Zhao, L., Zou, D. F., Hu, G., Du, E., Pang, Q., Xiao, Y., Li, R., Sheng, Y., Wu, X., Sun, Z., Wang, L., Wang, C., Ma, L., Zhou, H., and Liu, S.: Changing climate and the permafrost environment on the Qinghai–Tibet(Xizang) Plateau, Permafrost and Periglac Process, 1-10, https://doi.org/10.1002/ppp.2056, 2020.

Zou, D., Zhao, L., Sheng, Y., Chen, J., Hu, G., Wu, T., Wu, J., Xie, C., Wu, X., Pang, Q., Wang, W., Du, E., Li, W., Liu, G., Li, J., Qin, Y., Qiao, Y., Wang, Z., Shi, J., and Cheng, G.: A new map of permafrost distribution on the Tibetan Plateau, Cryosphere, 11, 2527-2542, https://doi.org/10.5194/tc-11-2527-2017, 2017.